Trans Indian Inst Met (2020) 73(5):1301–1309
https://doi.org/10.1007/s12666-020-01957-1

ORIGINAL ARTICLE

The Effect of Lamellar and Globular α-Phase on Mechanical Behavior of Strongly Textured Ti–6Al–4V alloy

Peyman Ahmadian[1] · **Maryam Morakabati**[1]

Received: 4 November 2019 / Accepted: 17 March 2020 / Published online: 6 May 2020

Abstract In this study, the effect of lamellar and globular α-phase on mechanical properties of strongly textured Ti–6Al–4V alloy was investigated. The strong transverse texture was developed in Ti–6Al–4V alloy via α + β rolling at 950 °C. In the following, lamellar and equiaxed microstructures have been separately promoted in the Ti–6Al–4V alloy during annealing at β- and α + β regions, respectively. According to EBSD analysis, it was revealed that deformation texture was not considerably changed during different annealing processes. Then, room temperature mechanical properties of the studied alloy including uniaxial tensile, compression and bending tests were evaluated. According to the tensile test, work hardening capacity was obtained as 1.10 and 0.64 for equiaxed and lamellar microstructures, respectively. Fracture limit curve revealed that equiaxed microstructure had more extent of homogeneous deformation in comparison with lamellar one. In addition, bending properties of the Ti–6Al–4V alloy were significantly improved as a result of equiaxed microstructure.

Keywords Ti–6Al–4V · α-Phase morphology · Work hardening capacity · Fracture limit curve · Bending properties

✉ Peyman Ahmadian
pahmadian7@gmail.com

✉ Maryam Morakabati
m_morakabati@mut.ac.ir

[1] Faculty of Material and Manufacturing Technologies, Malek Ashtar University of Technology, Tehran, Iran

1 Introduction

Ti–6Al–4V is one of the α + β titanium alloys. This alloy consists of dominant alpha phase and retained beta phase. The crystal structures of alpha and beta phase are hexagonal (a = 0.295 nm, c = 0.468 nm) and body-centered cubic (a = 0.332 nm), respectively [1]. Ti–6Al–4V was nominated as a work horse alloy in the family of titanium alloys. Excellent corrosion resistance [2], good fatigue [3] and creep properties [4], appropriate biocompatibility [5] and high specific strength (strength-to-density ratio) [6] convince various branches of industries to manipulate this alloy. Therefore, Ti–6Al–4V has its unique place in a considerable number of industries including aviation, aerospace, petroleum, medical, turbine, chemical, marine, etc. Despite noticeable advantages, cold workability of Ti–6Al–4V alloy is restricted [7]. Extensive researches reveal that mechanical properties of Ti–6Al–4V alloy are directly related to microstructure and crystallographic texture. For instance, the effect of α-phase morphology on micro-mechanical behavior of Ti–6Al–4V alloy has been investigated [8]. The results show that higher micro-hardness and ultimate tensile strength in Ti–6Al–4V alloys are achieved as a result of equiaxed microstructure. According to Matsumoto's research [9], annealing at α + β region and subsequent quenching results in appropriate room temperature tensile ductility. The effect of alpha phase texture component on deformation behavior of Ti–6Al–4V alloy has been reported in our previous researches [10, 11]. The results of tensile test show that transverse texture results in low yield stress in comparison with basal texture component [10]. Also, during uniaxial compression test of Ti–6Al–4V alloy, low resistance to deformation and high content of geometrically necessary dislocations are observed for transverse texture [11]. Also, we have studied

the effect of rolling temperature at α + β region on final cold workability of Ti–6Al–4V alloy [12]. The results indicate that increasing rolling temperature at α + β region is associated with promotion of transverse texture component and improvement in cold workability of Ti–6Al–4V alloy. It has been demonstrated that grain size of prior β-phase and the thickness of α-colony have significant effect on tensile properties of fully lamellar Ti–6Al–4V alloy [13]. The highest mechanical properties (σ_{UTS} = 1299 MPa and σ_{YS} = 1191 MPa) were obtained in Ti–6Al–4V alloy via warm rolling at 650 °C [14]. The main reason for this phenomenon is the formation of $\langle 10\bar{1}0\rangle//RD$ fiber during unidirectional warm rolling at 650 °C. According to the evidences that were found by Jiang et al. [15], it can be demonstrated that the value of anisotropy degree is decreased in titanium alloys as a result of $(\bar{1}013)[5\bar{2}\bar{3}0]$ texture promotion via cold rolling and subsequent annealing at 700 °C. The major microstructural factors that significantly control room temperature mechanical properties of Ti–6Al–4V alloy with initial bimodal microstructure were determined by Chong et al. [16]. In spite of the mentioned studies, the effect of lamellar and equiaxed α-phase on mechanical properties of Ti–6Al–4V alloy has not been comprehensively investigated. Therefore, it is necessary to investigate the effect of globular and lamellar α-phase on room temperature mechanical properties of Ti–6Al–4V alloy. For this purpose, initial transverse texture was developed in Ti–6Al–4V alloy via α + β rolling process. Then, fully equiaxed and fully lamellar microstructure were separately promoted in the strongly textured Ti–6Al–4V alloy. Finally, the effect of α-phase morphology on work hardening capacity was estimated using uniaxial tensile test. The degree of homogeneous deformation was investigated by fracture limit curve extracted from uniaxial compression data; bending properties of the studied alloy were measured using semi-guided bend test.

2 Materials and Experimental Procedures

Titanium sponge and aluminum–vanadium master alloy (60 Al–40 V) were compressed using hydraulic press in order to produce blocks with appropriate green strength. The blocks were welded together using argon gas. The produced first-melt electrodes were refined using vacuum arc remelting (VAR) process for three times. The chemical composition of the studied material (Ti, Al, V, Fe, C) was analyzed using atomic emission spectroscopy (metal analyzer M5000 S). Oxygen, nitrogen and hydrogen content was measured using gas analyzer (PerkinElmer series II 2400). The chemical composition of the studied alloy (Table 1) is in the permissible range of Ti–6Al–4V (grade 5) [17]. Transus temperature of the Ti–6Al–4V alloy was determined using annealing and quenching technique. According to this method, transus temperature of the studied alloys was determined to be in the range of 980–995 °C.

The schematic of the applied thermomechanical process is shown in Fig. 1. It is divided into four different steps: At the first step, the remelted ingot was homogenized at β-region (1100 ± 5 °C, stage I) for 4 h and subsequently quenched in the water. Then, primary and secondary hot rolling was unidirectionally performed at 1100 ± 10 °C (β-region, stage II) and 950 ± 10 °C (α + β region, stage III), respectively. The value of reduction during primary and secondary hot rolling was approximately 81% and 68%, respectively. The thickness of billet reached from 160 mm to 30 mm via primary hot rolling at β- region (1100 ± 10 °C). In the following, the final thickness of billet reached to 9.5 mm during secondary hot rolling at α + β region (950 ± 10 °C). The diameter and the speed of rollers were 500 mm and 1 rpm, respectively.

The macro-texture of the as-rolled Ti–6Al–4V alloy was measured using X-ray diffraction method. XRD analysis was done by Cu-K_α radiation (λ = 1.7928 A°). Pole figure plane of (0002), inverse pole figure and orientation distribution function (ODF) were calculated using the Mtex (MATLAB texture) software. Finally, two different heat treatment cycles were designed in order to obtain fully lamellar and fully equiaxed microstructures. The fully lamellar microstructure was obtained as a result of annealing at β-region (1050 ± 5 °C, stage IV) for 30 min and slow cooling at furnace (1 °C/min). In addition, annealing at α + β region (960 ± 5 °C, stage IV) for 30 min and subsequent furnace cooling (1 °C/min) resulted in fully equiaxed microstructure. The temperature tolerance of the specimens during different rolling and annealing processes was accurately measured using WIKA thermocouple. Optical microscopy images were obtained using conventional metallographic method using Kroll etchant. Also the micro-texture of the specimens was investigated using electron back-scattered diffraction. The detail of this technique was described in our previous research [10]. Then, mechanical properties of specimens including uniaxial tensile, compression and bending tests were investigated at room temperature. The schematic position of the specimens for mechanical tests is illustrated in Fig. 2. Tensile properties of specimens were measured according to ASTM E8 [18] using Instron-8502 machine. For each specimen, the tensile test was repeated five times and mean value and standard deviation were reported. It is obviously observed in Fig. 2 that the shape of the tensile specimen is flat and it is located in RD–ND plane. Also, the axis of the tensile specimen is located at the middle of RD–ND plane. The yield stress value was measured using 0.2%

Table 1 Chemical composition of the as-received Ti–6Al–4V alloy

Ti	Al	V	Fe	C	O (ppm)	N (ppm)	H (ppm)
Base	6.21	4.13	0.02	0.01	1000	53	89

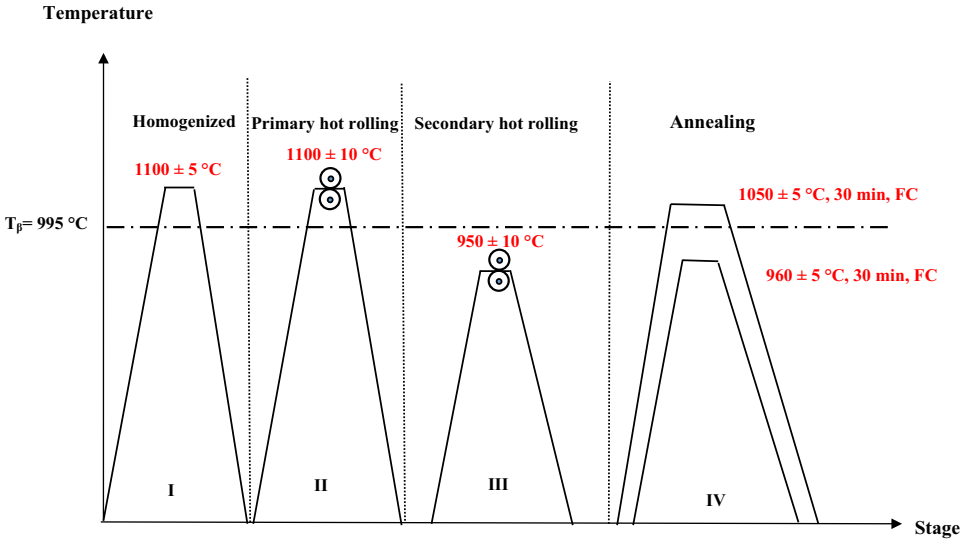

Fig. 1 Schematic of the thermomechanical process applied to the Ti–6Al–4V alloy

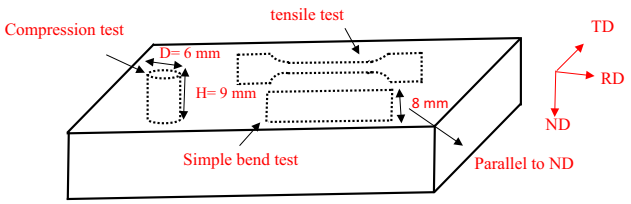

Fig. 2 Schematic illustration of specimens for compression, tensile and bending test

offset method. The cross-head velocity was 2 mm/min. The value of work hardening capacity (Hc) was computed for each sample based on tensile properties (i.e., ultimate tensile strength (σ_{UTS}), yield stress (σ_{YS}) and elongation (e)) using Eq. 1:

$$H_c = \left(\frac{\sigma_{UTS} - \sigma_{YS}}{\sigma_{UTS}}\right) \times (\%e) \quad (1)$$

The cylindrical specimens with the height (H) of 9 mm and diameter (D) of 6 mm (H:D = 1.5) were prepared for uniaxial compression test. The uniaxial compression tests were performed using the same tensile test machine and constant cross-head velocity of 0.5 mm/min. Finally, fracture limit diagram was derived for each specimen according to hoop and axial strains. The specimens with the dimension of 40 × 8 × 2 mm were prepared for simple bend test. Subsequently, semi-guided bend test was carried out according to ASTM E290 [19].

3 Result and Discussion

3.1 Texture and Microstructure Evolution

After secondary hot rolling at 950 °C (α + β region), the crystallographic texture of α-phase was computed using X-ray diffraction (Fig. 3a). (0002) pole figure, inverse pole figure and orientation distribution function (ODF) are illustrated in Fig. 3a–c, respectively. (0002) pole (Fig. 3a) indicates that during secondary hot rolling at α + β region (950 °C), α-phase crystals are rotated in such a way that strong transverse texture develops in the as-rolled Ti–6Al–4V alloy. The inverse pole figure map (Fig. 3b) presents that α-crystals are oriented toward $[10\bar{1}0]$ and $[11\bar{2}0]$ axis. Therefore, strong transverse texture develops in the Ti–6Al–4V alloy. According to previous studies [20, 21], it has been demonstrated that unidirectional rolling of dual-phase titanium alloys at α + β region is associated with transverse texture evolution which has adequate compatibility with our results about texture development in Ti–6Al–4V alloy. (0002) Pole figure provides incomplete data about orientation; so comprehensive three-dimensional data (based on Euler angle: $\varphi_1 - \phi - \varphi_2$) can be derived

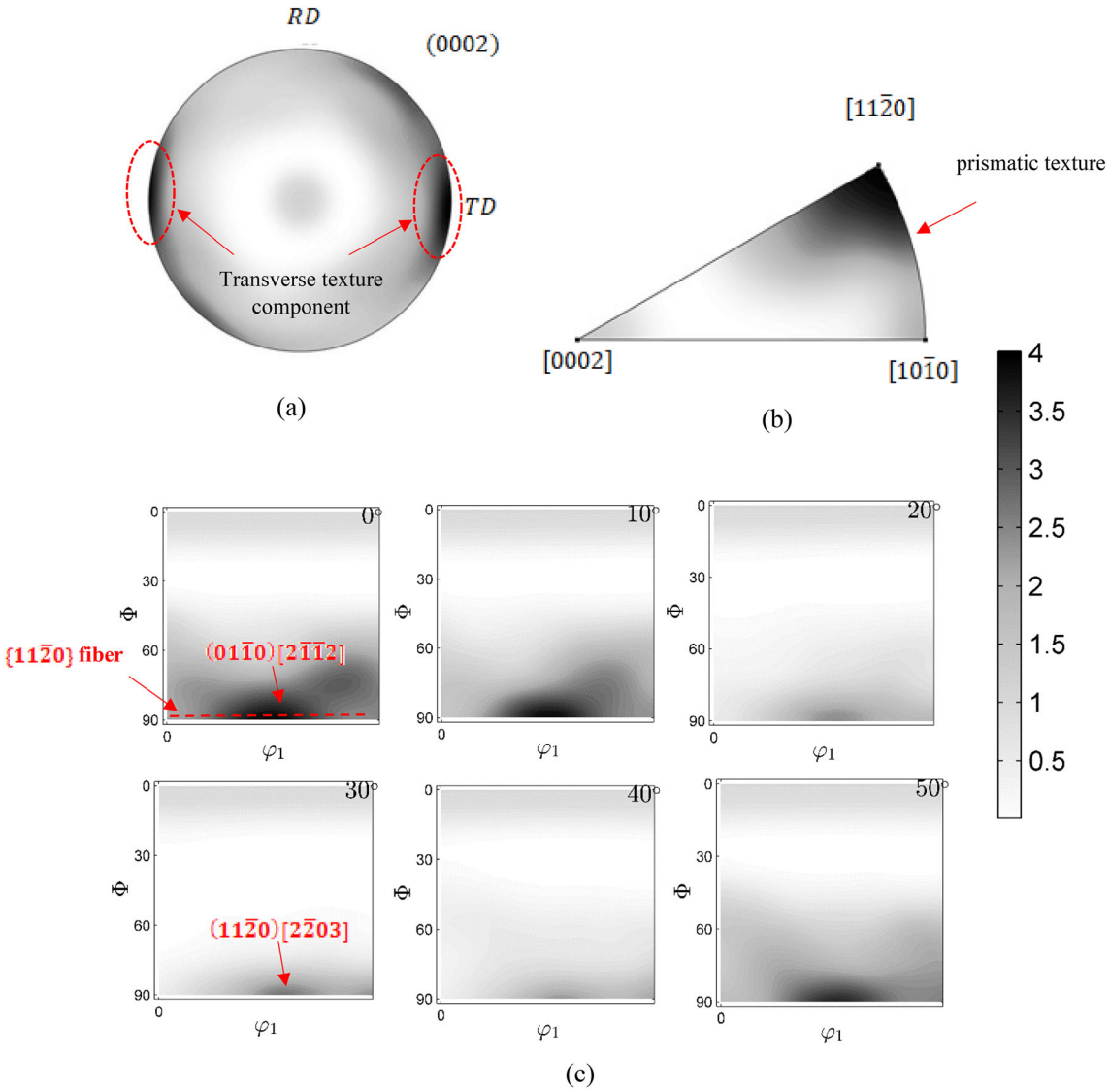

Fig. 3 Texture development in α-phase crystals via secondary hot rolling at 950 °C: **a** (0002) pole figure, **b** inverse pole figure, **c** orientation distribution function (ODF)

using orientation distribution function [22]. In Fig. 3c, the important texture component of Ti–6Al–4V alloy is presented by miller indices and fiber texture. Strong $(01\bar{1}0)[2\bar{1}\bar{1}2]$ texture component is observed at $\varphi_2 = 0°$ section. A weak $(11\bar{2}0)[2\bar{2}03]$ texture component also develops ($\varphi_2 = 30°$). It is obviously seen that $\{11\bar{2}0\}$ fiber ($\varphi_2 = 0°$) has been augmented in Ti–6Al–4V alloy as a result of hot rolling at α + β region (950 °C). The position of fiber textures on ODF sections was previously reported by Y.N. Wang et al. [23]. It was previously demonstrated that annealing process has inconsiderable effect on texture component of hexagonal metals, especially Ti–6Al–4V alloy [24]. Therefore, during annealing process, major microstructure of Ti–6Al–4V alloy recrystallizes without any changes in α-crystal's orientation.

The microstructure evolution during thermomechanical process is presented in Fig. 4. The microstructure of the Ti–6Al–4V alloy in as-rolled condition (Fig. 4a) indicates that α- and β-phases are elongated through rolling direction (RD). During secondary rolling at α + β region (950 °C), some degree of the β-phase concurrently transforms to the α-phase. Therefore, predominant α-phase and retained β-phase, located between α-platelets, are observed. According to Clemex analysis, it is found that the volume fraction of predominant α- and retained β-phase are 81% and 19%, respectively. Also, the mean thickness of α-lamella is 3.7 ± 0.25 μm. Similar result about the influence of β-process on microstructural parameters of Ti–6Al–4V alloy was reported by Shi et al. [13]. The effect of annealing condition on microstructure evolution of the Ti–6Al–4V

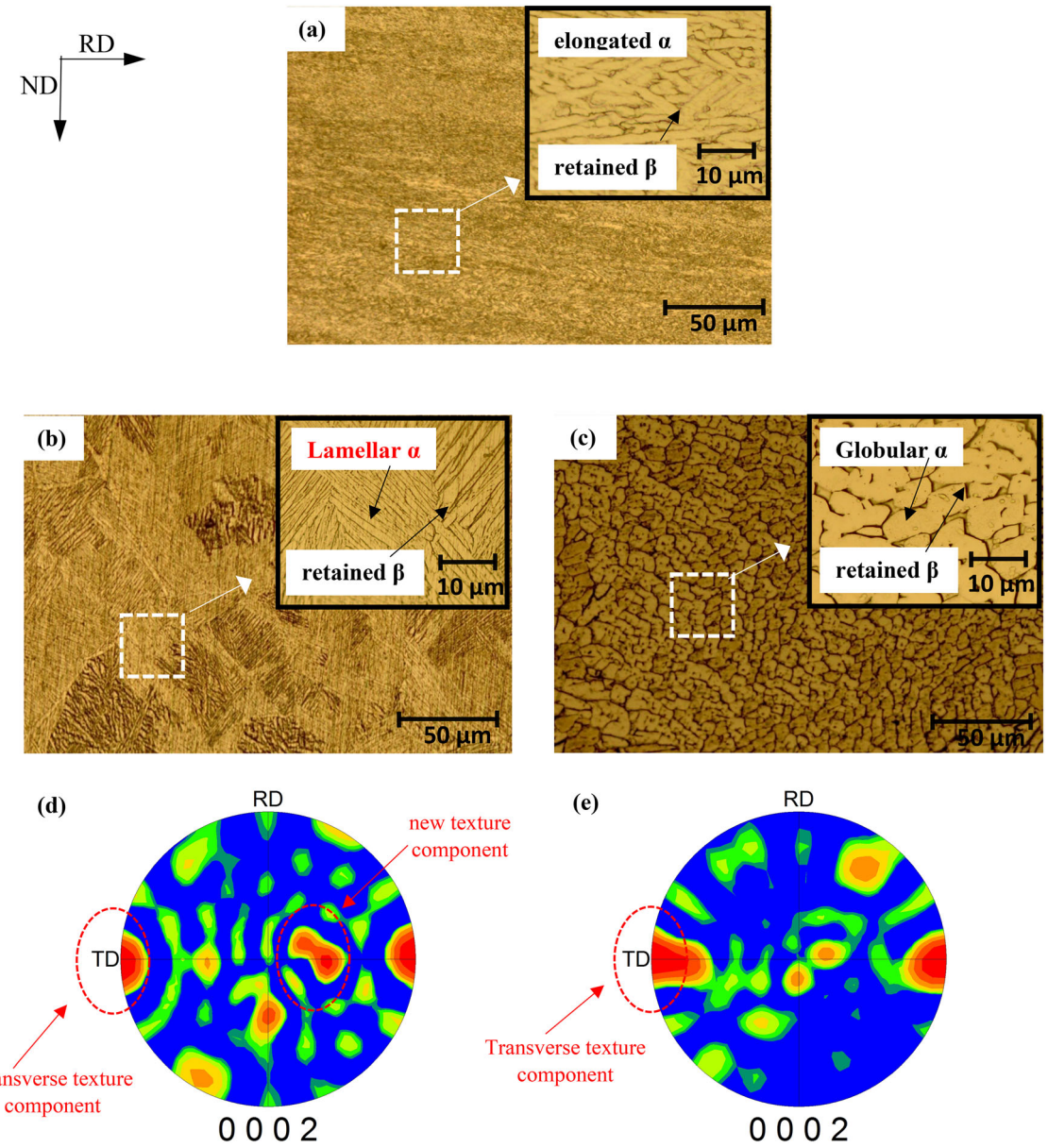

Fig. 4 Microstructure and micro-texture evolution during annealing process: **a** as-rolled microstructure after secondary at 950 °C, **b** annealing at 1050 °C, 30 min, furnace cooling (1 °C/min), **c** annealing at 960 °C, 30 min, furnace cooling (1 °C/min), **d** (0002) pole figure of α-phase after annealing at 1050 °C, **e** (0002) pole figure of α-phase after annealing at 960 °C. Kroll etchant (3% HF + 6% HNO_3 + distilled water) was used for microstructure observation

alloy is presented in Fig. 4b and c. Ding et al. [25] demonstrated that the morphology of lamellar α-phase directly depends on cooling rate. During β-annealing of Ti–6Al–4V alloy, colonized plate-like α, basket weave and Widmanstätten morphology is expected as a result of low, medium and high cooling rates, respectively. As shown in Fig. 4b, the fully lamellar microstructure is produced in the Ti–6Al–4V alloy as a result of annealing at 1050 °C and subsequent cooling in the furnace (1 °C/min). The retained β is surrounded by dominant plate-like α-phase. The volume fraction of α- and β-phase is 79% and 21%, respectively. Therefore, during β-annealing process, the volume fraction of α- and β-component does not significantly changes in comparison with as-rolled state. Also, the mean thickness of α-lamella decreases from 3.7 ± 0.25 μm (in as-rolled state) to 2.9 ± 0.21 μm (in β-annealed state). As

shown in Fig. 4c, primary α-phase has grown as a result of annealing at 960 °C. The lamellae α-phase is not formed, and retained β-phase is located between triple points of globular α-grains with mean size of 4.3 ± 0.17 μm. Therefore, the resulting microstructure is equiaxed with equilibrium volume fraction of α- and β-phase. The volume fraction of α- and β-phase for obtained equiaxed microstructure is, respectively, 91% and 9% which is compatible with other research [1]. The effect of annealing process on texture evolution of Ti–6Al–4V alloy has been investigated using electron back-scattered analysis. The strong transverse texture is obviously observed as a result of annealing at 1050 °C (Fig. 4d) and 960 °C (Fig. 4e). Transverse texture component initially develops in Ti–6Al–4V alloy during α + β rolling stage (Fig. 3). In the case of annealing at 1050 °C and subsequent cooling from β-region, other texture component is weakly promoted which is associated with variant selection during α → β transformation (Fig. 4d) [24]. In spite of some new texture component development during annealing process, it can be certainly demonstrated that transverse texture completely remains in β- and α + β-annealed specimens. In the following, the effect of α-phase morphology (plate-like and globular) with initial transverse texture on mechanical response of the Ti–6Al–4V alloy has been investigated.

3.2 α-Phase Morphology and Tensile Properties of Ti–6Al–4V

The effect of α-phase morphology on tensile behavior of the Ti–6Al–4V alloy is reported in Fig. 5 and Table 2. Because of similar crystallographic texture, it can be certainly declared that tensile behavior of the Ti–6Al–4V alloy is significantly related to effective slip length of α-phase. In the case of plate-like and globular α-phase, effective slip length magnitude is determined by the thickness of lamellae and grain size of globular α-phase, respectively. Through plastic deformation, α- and β-phases are deformed individually. Hence, different slip systems are activated in both α- and β-phases. Lutjering [1] mentioned that two slip systems are exactly parallel (i.e., $(110)[1\bar{1}1]_{\beta}//(0002)[11\bar{2}0]_{\alpha}$ and $(\bar{1}12)[1\bar{1}1]_{\beta}//(\bar{1}100)[11\bar{2}0])_{\alpha}$ and there is only 10° misorientation between two other important slip systems (i.e., $(110)[1\bar{1}2]_{\beta}$ and $(0002)[1\bar{2}10]_{\alpha}$ as well as $(1\bar{1}2)[\bar{1}11]_{\beta}$ and $(10\bar{1}0)[1\bar{2}10]_{\alpha}$). Therefore, regarding the same crystallographic texture, it can be demonstrated that the morphology of α-phase has significant effect on dislocation transformation across the incoherent α/β interface. According to Fig. 5, it is clearly observed that the value of strain at fracture point in specimen with initial equiaxed microstructure is higher than lamellar one. It was previously reported [16] that in Ti–6Al–4V alloy, the value of elongation during uniaxial tensile test is directly related to volume fraction of globular α-phase. In addition, the area below the strain–stress curve for equiaxed and lamellar microstructures is 149 MPa. mm/mm and 128 MPa. mm/mm, respectively. Therefore, higher toughness and higher crack propagation resistance are expected for specimen with globular α-phase in comparison with plate-like morphology. The effect of α-phase morphology on work hardening capacity has been evaluated using H_c parameter (Eq. 1). According to tensile data (Table 2), it can be demonstrated that globular α-phase improves work

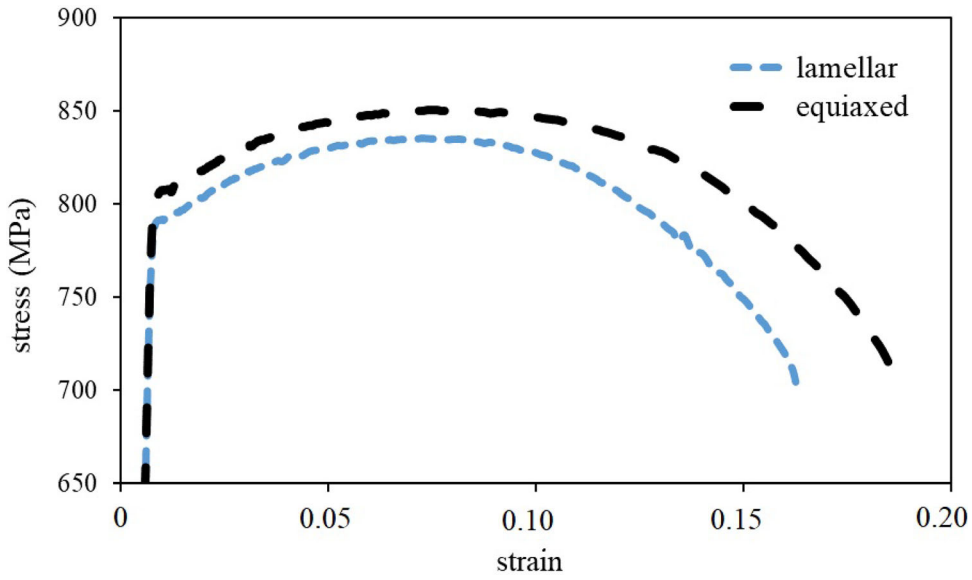

Fig. 5 Stress–strain curve of the Ti–6Al–4V alloy for lamellar and equiaxed microstructure with the same transverse texture

Table 2 Effect of initial microstructure on tensile properties of the **Ti–6Al–4V** alloy

Microstructure	UTS (MPa)		YS (MPa)		Elongation		Work hardening capacity
	Mean	SD	Mean	SD	Mean	SD	
Equiaxed	853.3	13.1	802.8	21.5	18.4	2.5	1.10
Lamellar	833.5	14.3	798.5	19.8	15.3	2.7	0.64

SD standard deviation

hardening capacity in the Ti–6Al–4V alloy. The value of work hardening capacity (H_c) for equiaxed and lamellar microstructures is obtained as 1.10 and 0.64, respectively.

3.3 α-Phase Morphology and Bending Properties of Ti–6Al–4V

In the following, the effect of initial microstructure on bending capacity of The Ti–6Al–4V alloy has been evaluated with plate-like ones.

In Fig. 6, globular α-phase retards crack nucleation and propagation; hence, the specimen with initial equiaxed microstructure endures more level of bending before crack initiation. The result of bending test indicates that microcrack is observed in the specimen with initial lamellar microstructure after 30° bending, while after 90° bending, the microcrack does not appear in the specimen with initial equiaxed microstructure. Similar to the tensile test, it can be demonstrated that globular α-phase reveals more resistance to crack propagation in comparison with plate-like ones.

3.4 α-Phase Morphology and Compression Properties of Ti–6Al–4V

The effect of α-phase morphology on the degree of homogeneity of deformation has been expressed using fracture limit curve (Fig. 7). Fracture limit curve is extracted using uniaxial compression test. In Fig. 7a, the schematic image of homogeneous and nonhomogeneous deformation during upset test has been illustrated. The value of stress in radius direction ($\sigma_r = 0$) is zero for both homogeneous and nonhomogeneous deformations. In the case of homogeneous state, the hoop stress (σ_θ) is zero. Therefore, no bulging occurs during deformation. However, in nonhomogeneous deformation, bulging occurs as a result of hoop stress. Hence, during uniaxial compression of the Ti–6Al–4V alloy, more hoop stress leads to sooner occurrence of bulging. In this study, the ratio between hoop stress (σ_θ) and axial stress (σ_z) has been manipulated as a quantitative criterion for estimating of homogeneity of deformation. Therefore, η parameter is defined as follows (Eq. 2.):

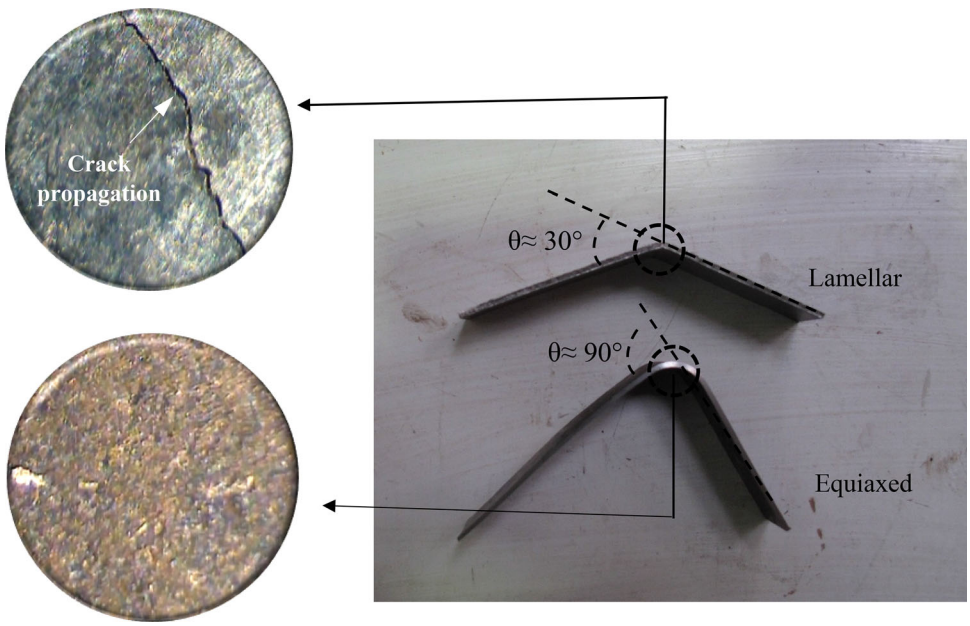

Fig. 6 Effect of α-phase morphology on bendability of the Ti–6Al–4V alloy

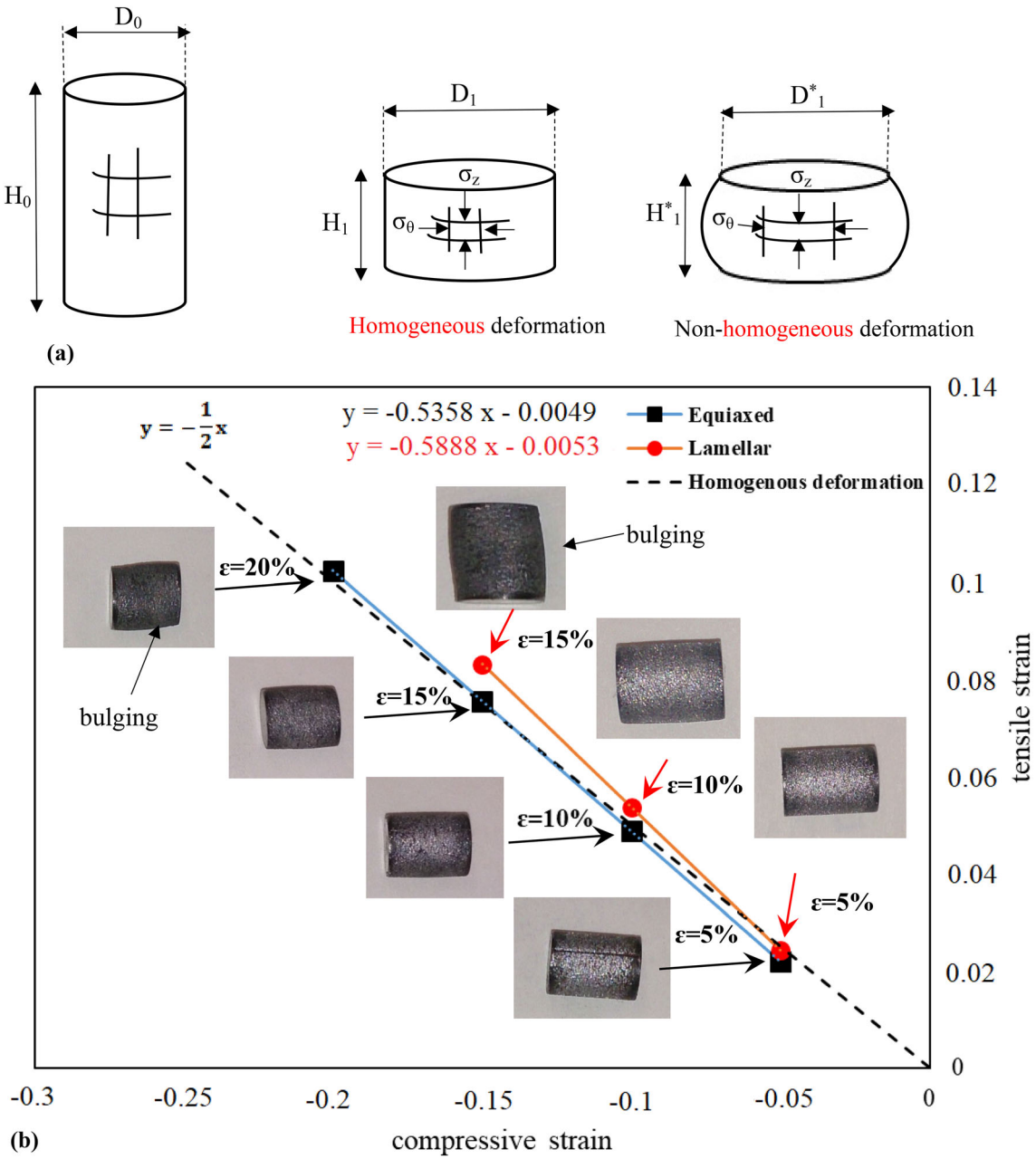

Fig. 7 **a** Schematic image of homogeneous and nonhomogeneous deformation during upset test. **b** Fracture limit curve during uniaxial compression test of the Ti–6Al–4V alloy

$$\eta = \frac{\sigma_\theta}{\sigma_z} \tag{2}$$

The specimens are assumed to have isotropic behavior. Therefore, the relationship between stress and strain in plastic region can be defined using Levy–Mises equation [26] (Eq. 3):

$$\begin{aligned} \mathrm{d}\varepsilon_\theta &= d_\lambda\left[\sigma_\theta - \left(\frac{\sigma_r + \sigma_z}{2}\right)\right] \\ \mathrm{d}\varepsilon_z &= d_\lambda\left[\sigma_z - \left(\frac{\sigma_\theta + \sigma_r}{2}\right)\right] \\ \mathrm{d}\varepsilon_r &= d_\lambda\left[\sigma_r - \left(\frac{\sigma_\theta + \sigma_z}{2}\right)\right] \end{aligned} \tag{3}$$

The value of strain has been experimentally calculated using deformed sample. In Fig. 7b, the stain path (i.e., tensile strain vs compressive strain) has been extracted for

the Ti–6Al–4V alloy with lamellar and equiaxed microstructures. The ratio between axial strain (compression strain) and hoop strain (tensile strain) is defined by γ parameter $\left(\gamma = \frac{d\varepsilon_z}{d\varepsilon_\theta}\right)$. Combining Eqs. 2 and 3 and considering no stress in radius direction ($\sigma_r = 0$), Eq. 4 is obtained as follows:

$$\eta = \frac{\gamma + 2}{2\gamma + 1} \tag{4}$$

In the case of homogeneous deformation, the value of η and γ are 0 and − 2, respectively [27]. The slopes of fracture limit curve $\left(\frac{d\varepsilon_\theta}{d\varepsilon_z}\right)$ for equiaxed and lamellar microstructures are obtained as − 0.53 and − 0.58, respectively (Fig. 7b). Therefore, the value of γ parameter for globular and plate-like α-phase through uniaxial compression test is calculated as − 1.86 and − 1.69, respectively. According to Eq. 4, the values of η parameter for equiaxed and lamellar microstructures are calculated as − 0.04 and − 0.12, respectively. Hence, the fracture limit curves indicate that through uniaxial compression test, more tensile stress (hoop stress) is generated at the specimen with initial lamellar microstructure. Therefore, bulging is observed at low level of strain (ε = 15%) in comparison with equiaxed microstructure (ε = 20%). Kulkarni et al. [28] demonstrated that during uniaxial compression of Ti–6Al–4V alloy, work hardening occurs as a result of α-phase fragmentation. This phenomenon is clearly observed in our study in the specimens with initial equiaxed and lamellar microstructure. Hence, it can be demonstrated that globular α-phase is associated with more homogeneous deformation in comparison with plate-like morphology.

4 Conclusion

The effect of lamellar and globular α-phase morphology on mechanical response of the strongly textured Ti–6Al–4V alloy was investigated. Strong transverse texture was developed in Ti–6Al–4V alloy via secondary hot rolling at 950 °C. Then, fully lamellar and equiaxed microstructures were separately formed as a result of annealing at β (1050 °C) and α + β (960 °C) region, respectively. Tensile test revealed that work hardening capacities for equiaxed and lamellar microstructures were 1.10 and 0.64, respectively. Also, bending test result showed that globular α-phase had higher resistance to crack propagation in comparison with lamellar microstructure. Through uniaxial compression test, low level of hoop stress (tensile stress) was generated at the specimen with globular α-phase. Therefore, bulging retarded and specimen deformed homogeneously as a result of equiaxed microstructure.

References

1. Lütjering G, and Williams J C, *Titanium*, Springer, Berlin (2007), p 203.
2. Zhao B, Wang H, Qiao N, Wang C, and M. Hu, *Mater Sci Eng C Mater Biol Appl* **70** (2017) 832.
3. Morrissey R J, and Nicholas T, *Int J Fatigue* **27** (2005) 1608.
4. Barboza M, Perez E, Medeiros M, Reis D, Nono M, Neto F P, and Silva C, *Mater Sci Eng A* **428** (2006) 319.
5. Nayar P, Bohm E, Petrak M, Caley W, and Cahoon J, *Can Metall* **55** (2016) 420.
6. Cheng X, Li S, Murr L, Zhang Z, Hao Y, Yang R, Medina F, and Wicker R, *J Mech Behav Biomed* **16** (2012) 153.
7. Gupta R, Kumar V A, Mathew C, and Rao G S, *Mater Sci Eng A* **662** (2016) 537.
8. Ma X, Li F, Li J, Cao J, Li P, and Dong J, *J Mater Eng Perform* **24** (2015) 3761.
9. Matsumoto H, Yoneda H, Sato K, Kurosu S, Maire E, Fabregue D, Konno T J, and Chiba A, *Mater Sci Eng A* **528** (2011) 1512.
10. Ahmadian P, Abbasi S M, and Morakabati M, *Mater Today Commun* **13** (2017) 332.
11. Ahmadian P, Abbasi S M, and Morakabati M, *Mater Today Commun* **14** (2018) 263.
12. Ahmadian P, Morakabati M, and Abbasi S M, *Int J Mater Res* **110** (2019) 543.
13. Shi X, Zeng W, Sun Y, Han Y, Zhao Y, and Guo P, *J Mater Eng Perform* **24** (2015) 1754.
14. Murty S N, Nayan N, Kumar P, Narayanan P R, Sharma S, and George K M, *Mater Sci Eng A* **589** (2014) 174.
15. Jiang H T, Liu J X, Mi Z L, Zhao A M, and Bi Y J, *Int J Min Met Mater* **19** (2012) 530.
16. Chong Y, Bhattacharjee T, Park M H, Shibata A, and Tsuji N, *Mater Sci Eng A* **730** (2018) 217.
17. Welsch G, Boyer R, and Collings E, *Material Properties Handbook: Titanium alloys*, ASM international, Ohio (1993), p 483.
18. ASTM E8/E8M-16a, Standard Test Methods for Tension Testing of Metallic Materials, (2016).
19. ASTM E290-14, Standard Test Methods for Bend Testing of Material for Ductility, (2014).
20. Chao Q, Hodgson P D, and Beladi H, *Metall Mater Trans A* **47** (2016) 531.
21. Lin P, Feng A, Yuan S, Li G, and Shen J, *Mater Sci Eng A* **563** (2013) 16.
22. Randle V, and Engler O, *Introduction to Texture Analysis: Macrotexture, Microtexture and Orientation Mapping*, CRC press, Florida (2014), p 75.
23. Wang Y, and Huang J, *Mater Chem Phys* **81** (2003) 11.
24. Obasi G C, Variant selection and its effect on texture in Ti–6Al–4V alloy, Ph.D. thesis, University of Manchester, England (2011).
25. Ding R, Guo Z, and Wilson A, *Mater Sci Eng A* **327** (2002) 233.
26. Hosford W F, and Caddell R M, *Metal Forming Mechanics and Metallurgy*, Cambridge University Press, Cambridge (2011), p 17.
27. Dieter G E, Kuhn H A, and Semiatin S L, *Handbook of Workability and Process Design*, ASM International, Ohio (2003), p 45.
28. Kulkarni G, Hiwarkar V, Patil J, and Singh R, *J Nanosci Nanotechnol Res* **2** (2018) 1.